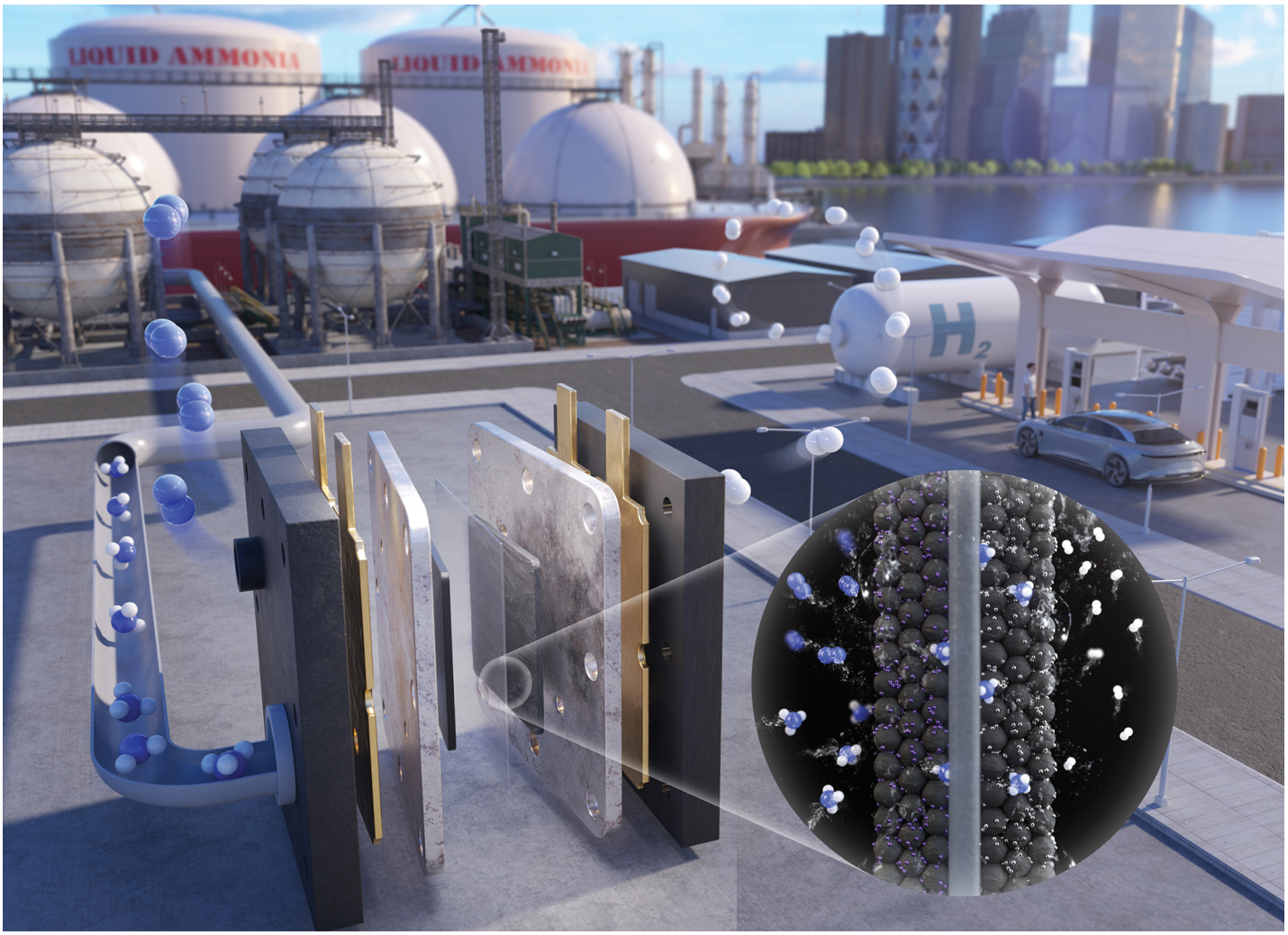

Showcasing research from Prof. Chang Won Yoon's lab., Pohang University of Science and Technology, Republic of Korea.

Direct electrolysis of liquid anhydrous ammonia for continuous production of high-purity, pressurized hydrogen at ambient temperature

NH_3 is valued as a large-scale H_2 carrier due to its high H_2 storage capacities (≥108 kg-H_2 m^{-3}, 17.7 wt%) and simple liquefaction conditions (25 °C at 10 bar). However, producing high-purity and pressurized H_2 *via* catalytic NH_3(g) thermolysis requires high temperatures (>600 °C) with multiple purification and compression steps. Here, we present a proof-of-concept study using a zero-gap liquid anhydrous NH_3 electrolyzer comprising electrocatalysts and a cation exchange membrane that directly converts gap liquid anhydrous NH_3 into high-purity (>99.99%) and pressurized (>5.5 bar) H_2 at 10 °C with a Faradaic efficiency of >98.8%.

Image reproduced by permission of Chang Won Yoon from *EES Catal.*, 2025, **3**, 694.

As featured in:

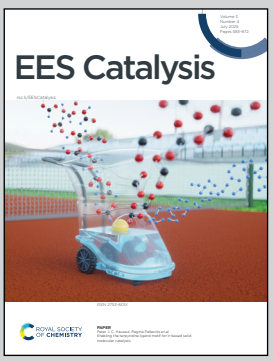

See Chang Won Yoon *et al.*, *EES Catal.*, 2025, **3**, 694.

ROYAL SOCIETY OF CHEMISTRY

rsc.li/EESCatalysis

Registered charity number: 207890

EES Catalysis

COMMUNICATION

View Article Online
View Journal | View Issue

Cite this: *EES Catal.*, 2025, 3, 694

Received 11th May 2025,
Accepted 14th May 2025

DOI: 10.1039/d5ey00140d

rsc.li/eescatalysis

Direct electrolysis of liquid anhydrous ammonia for continuous production of high-purity, pressurized hydrogen at ambient temperature†

Seungmok Han,[ab] Junsoo Ha,[a] Jae Seung Lee,[a] Hyukjoo Lee,[c] Chang Hyun Lee,[c] Kangwoo Cho[b] and Chang Won Yoon*[a]

The direct electrolysis of liquid anhydrous ammonia (NH_3(l), >99.99% of NH_3, free of water and solvent) is demonstrated using a 25 cm^2 zero-gap electrolyzer, consisting of a Ru/C anode and a Pt/C cathode, with the two electrodes spatially separated by a cation exchange membrane. This system, supplied by NH_3(l) and NH_4Br as the supporting electrolyte, continuously produces high-purity and pressurized hydrogen (H_2, >99.99%, >5.5 bar) at a temperature of 10 °C and a pressure of 6.2 bar, without requiring H_2/N_2 separation and compression processes. The direct NH_3(l) electrolyzer exhibits a cell potential of 1.1 V at 0.1 A cm^{-2}, presenting a faradaic efficiency of >99.3% for H_2 production. The developed system achieves a H_2 production rate of >18.8 mol-H_2 g_{cat}^{-1} h^{-1} at 0.5 A cm^{-2}, which is 4.7-fold higher than the highest H_2 production rate reported to date for NH_3(g) thermolysis at temperatures of over 500 °C.

Broader context

Hydrogen (H_2) is a key energy carrier that resolves the imbalance between renewable energy production and demand, contributing to global carbon neutrality. However, the low volumetric energy density of gaseous H_2 (3 kWh m^{-3} at 20 °C, 1 bar) poses challenges for large-scale storage and transportation. To address this limitation, ammonia (NH_3) has gained significant attention as a sustainable H_2 carrier due to its superior H_2 storage capacity and simple liquefaction conditions (10 bar at 25 °C). NH_3(g) thermolysis for hydrogen production is currently being developed for commercial implementation, but it requires high reaction temperatures (>600 °C) with multi-step purification, separation and compression processes. This study presents a proof-of-concept demonstration of the direct electrolysis of liquid anhydrous NH_3 (>99.99%, water/solvent-free) to produce H_2 at near-ambient temperature (10 °C). The zero-gap NH_3(l) electrolyzer, designed with electrocatalysts and a cation exchange membrane, enables the production of high-purity (>99.99%) and pressurized (>5.5 bar) H_2 in a single process. Our developed system achieves a faradaic efficiency of >98.8% and a 4.7-fold higher H_2 production rate compared to the state-of-the-art NH_3(g) thermolysis. The proposed continuous NH_3(l) electrolyzer offers an alternative H_2 production model from NH_3, potentially improving the cost efficiency and flexibility of H_2 generation facilities.

Introduction

Hydrogen (H_2) is a promising renewable energy carrier owing to its high gravimetric energy density (33.3 kWh kg-H_2^{-1}) and environmentally benign properties. However, its low volumetric energy density (3 kWh m^{-3} at 20 °C, 1 bar) poses a substantial scientific challenge, particularly for its large-scale storage and long-distance transportation.[1–3] To address these limitations, green and/or blue ammonia (NH_3) has been proposed as a promising H_2 carrier due to its high volumetric H_2 storage capacity (≥108 kg-H_2 m^{-3}),[4–7] and ease of liquefaction (*e.g.*, 25 °C, 10 bar). The transported liquid anhydrous NH_3 (NH_3(l), >99.99% of NH_3, free of water and solvent) can then release H_2 on demand through thermal cracking, releasing only nitrogen (N_2) as a byproduct, as shown in eqn (1). However, due to its endothermic nature, most of the processes currently being developed to thermally crack NH_3(g) typically require high temperatures exceeding 600 °C and even higher temperatures are needed to obtain high-pressure H_2.[8] Accordingly, a thermally enhanced NH_3(g) dehydrogenation process integrated with multistep separation procedures may be suitable for a centralized H_2 production facility (Fig. 1A).[9,10]

$$NH_3 \rightarrow 0.5N_2 + 1.5H_2, \quad \Delta H = +46\ \text{kJ mol}^{-1} \qquad (1)$$

$$NH_3(l) \rightarrow 0.5N_2 + 1.5H_2, \quad E = 0.068\ \text{V} \qquad (2)$$

As an alternative strategy, electrochemically converting NH_3 to H_2 has been proposed. Two concepts for the electrolysis of NH_3 exist: (i) aqueous NH_3 electro-oxidation reaction (AOR, NH_3(aq), Fig. 1B)[11–13] and (ii) direct electrolysis of liquid

[a] *Department of Chemical Engineering, Pohang University of Science and Technology (POSTECH), Pohang, 37673, Republic of Korea. E-mail: cwyoon@postech.ac.kr*
[b] *Division of Environmental Science and Engineering, Pohang University of Science and Technology (POSTECH), Pohang, 37673, Republic of Korea*
[c] *Department of Energy Engineering, Dankook University, Cheonan, 31116, Republic of Korea*

† Electronic supplementary information (ESI) available: Document S1: equations of ammonia electro-oxidation reaction S1–S3, Notes S1–S4, Fig. S1–S12, Tables S1–S3 and references. See DOI: https://doi.org/10.1039/d5ey00140d

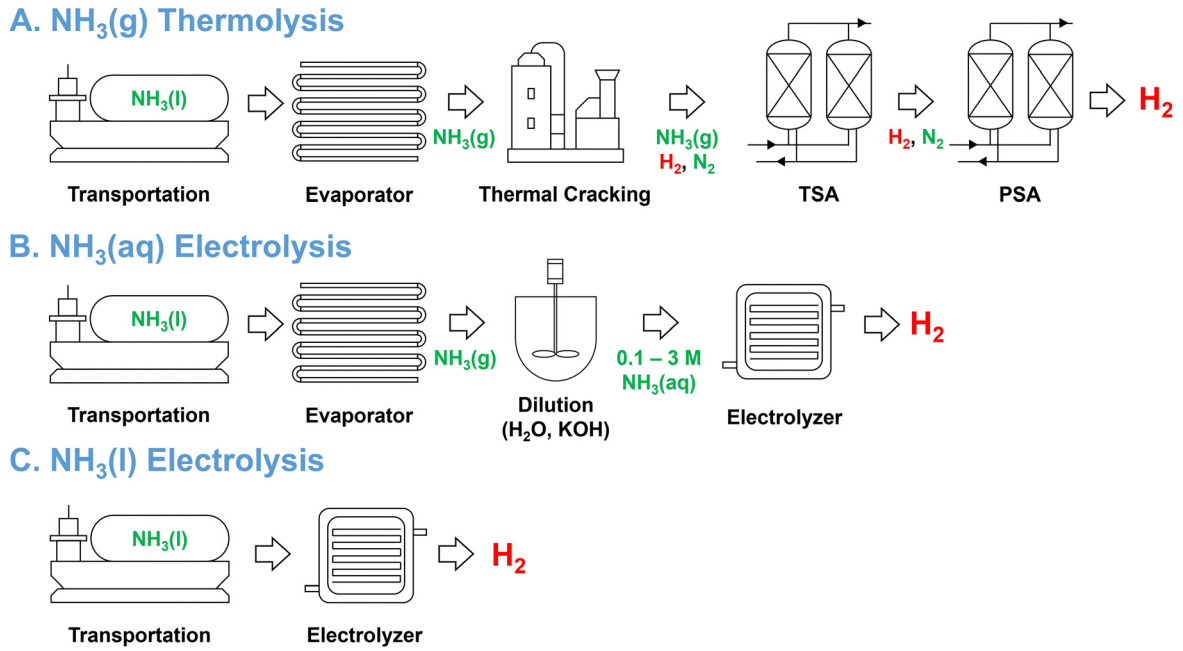

Fig. 1 **Schematic illustration of three H_2 production methods utilizing NH_3.** (A) Thermolysis of NH_3(g). (B) Ammonia electro-oxidation reaction (AOR) of diluted NH_3(aq). (C) Direct electrolysis of NH_3(l).

anhydrous NH_3 (NH_3(l), Fig. 1C).[14–17] Compared with the potential of water electrolysis (+1.23 V),[18,19] these methods lower the cell voltage (E_{cell}) to 0.060 V for the AOR (eqn (S1)–(S3), ESI†) and 0.068 V for direct NH_3(l) electrolysis (eqn (2) and Note S1, ESI†), thereby potentially achieving high energy efficiency for H_2 production. For the AOR, however, diluted aqueous NH_3(aq) solutions (*ca.* 0.1–3 M, 0.2–5 wt%) with potassium hydroxide (KOH, *ca.* 0.1–7 M, 0.6–30 wt%) in distilled H_2O are commonly used,[20–22] which require additional chemicals and waste treatment facilities, thus potentially increasing the cost of H_2 production. In addition, anodic N_2 production in the AOR competes with the oxygen evolution reaction in water electrolysis, possibly leading to the formation of byproducts such as NO_x.[23,24] Thus, cell operation at a high current density is limited, making it challenging to achieve a high H_2 production rate.

In contrast, direct NH_3(l) electrolysis requires no water addition and can be conducted under ambient temperature. In addition, NH_3(l) has favorable liquefaction conditions (25 °C at 10 bar) and appropriate viscosity (1.57 mPa s at 20 °C) for electrolysis.[25] Moreover, the volumetric and gravimetric H_2 storage capacities of NH_3(l) are higher than those of H_2O (112 kg-H_2 m^{-3} and 11.2 wt%). Previously, pioneering studies on NH_3(l) electrolysis using metal plates or disks in a batch reactor by adding either anionic (KNH_2, $NaNH_2$) or cationic (NH_4PF_6) supporting electrolyte have been shown to achieve H_2 generation.[14–16] However, the basic electrochemical properties (*e.g.*, anode/cathode potentials, overpotential and Tafel slopes) of the active metals used for NH_3(l) electrolysis have not been elucidated. Moreover, separation processes for the produced H_2/N_2 mixed gases are still necessary to obtain high-purity H_2 due to the limitations of batch reactions on small scales. Therefore, designing an efficient and scalable electrolysis system that enables the continuous production of high-purity H_2 in a flow reactor and acquiring fundamental parameters associated with NH_3(l) electrochemical reactions is necessary.

Here, we describe a continuous system for the direct electrolysis of NH_3(l) to produce high-purity and pressurized H_2. Potential anode and cathode active metals are initially screened in a batch reactor. Subsequently, a zero-gap type electrolysis cell, configured with a Ru/C anode and Pt/C cathode, each with an active area of 25 cm^2 on carbon foam and NH_4Br as a supporting electrolyte, is designed and operated under near-ambient temperature and pressurized conditions (10 °C, 6.2 bar). The developed electrochemical splitting system utilizing NH_3(l) demonstrates the continuous production of high-purity and pressurized H_2 (>99.99%, >5.5 bar) without a H_2/N_2 separation process, achieving a faradaic efficiency of >98.8% for H_2 production.

Results and discussion

$$\text{Anode (NER): } 4NH_3(l) \rightarrow 0.5N_2 + 3NH_4^+ + 3e^-, \quad E = 0.041 \text{ V } \textit{vs.} \text{ SHE} \tag{3}$$

$$\text{Cathode (HER): } 3NH_4^+ + 3e^- \rightarrow 1.5H_2 + 3NH_3(l), \quad E = -0.018 \text{ V } \textit{vs.} \text{ SHE} \tag{4}$$

$$K_{eq} \text{ of } 2NH_3(l) \leftrightarrow [NH_4^+][NH_2^-] = 10^{-33} \text{ (223 K)} \tag{5}$$

Because most of the electrochemical reactions studied to date are defined in aqueous media, calculating the theoretical potentials of the N_2 (nitrogen evolution reaction: NER) and H_2 (hydrogen evolution reaction: HER) evolution reactions for the direct electrolysis of NH_3(l) is necessary. When the partial

pressures of H_2 and N_2 are considered, the theoretical potentials for the NER and HER in the batch system are calculated as 0.041 and −0.018 V (eqn (3), (4) and Note S1–S3, ESI†), respectively, yielding an overall cell potential of 0.059 V. To screen potential catalysts for the electrolysis of NH_3(l), we initially design a semi-batch reactor using NH_4Br (1 M) as a supporting electrolyte (Fig. S1, ESI†) in NH_3(l) media. In this system, ammonium ions (NH_4^+) serves as a charge carrier and acts as a conjugated acid due to the autoionization property of NH_3(l) into NH_4^+ and amide ions (NH_2^-) (eqn (5)), similar to water ($2H_2O \rightarrow H_3O^+ + OH^-$). Standard electrodes are fabricated using various commercial metal species (Pt, Ru, Pd, Ni, Fe and Co) on carbon. High-angle annular dark-field scanning transmission electron microscopy (HAADF-STEM) analyses indicate that the uniformly distributed Pt, Ru and Pd nanoparticles have average sizes of 2.1, 2.8 and 3.7 nm, respectively, while Ni, Fe and Co metals exist as aggregated forms with sizes of >6 nm (Fig. S2, ESI†).

$$NH_3 \rightarrow NH_2^* + H^* \quad (6)$$

$$N^* + N^* \rightarrow N_2 + 2^* \quad (7)$$

The catalytic activities of the prepared electrodes are then determined based on overpotentials (η) and Tafel slopes obtained from linear sweep voltammograms (LSVs). The electrolysis conditions of 6.2 bar and 10 °C are selected to maintain the liquid state of NH_3 during the reaction. For the NER, among the screened metals, the Ru electrode exhibits the highest activity with the lowest overpotential (η = 489 mV at 10 mA cm^{-2}, 829 mV at 50 mA cm^{-2}, 1113 mV at 100 mA cm^{-2}, with *iR*-compensation) (Fig. 2A and Fig. S3A, ESI†). The overpotential at 10 mA cm^{-2} in NH_3(l) electrolysis is higher compared to that observed in water electrolysis using Ru/C (<400 mV at 10 mA cm^{-2}).[26,27] In addition, the high Tafel slope of Ru/C (381 mV dec^{-1}, Fig. S3B, ESI†) further indicates the sluggish kinetics of the NER. Note that the Ru catalyst in the NER electrode undergoes gradual deactivation over time due to nitriding and metal dissolution (Fig. S4 and Table S1, ESI†), consistent with a previous report.[28] Nonetheless, the relatively high activity of Ru/C could likely be associated with the capability of Ru metal to promote both N–H bond scission (eqn (6)) and associative N_2 desorption (eqn (7)), as proposed by previous reports.[29,30] Consistently, Hansgen *et al.* reported that Ru metals facilitate the reaction steps of N–H scission and associative N_2 desorption, which are the rate-determining steps of NH_3 decomposition.[31]

Then, we further screen potential HER electrocatalysts, demonstrating that the activities toward H_2 evolution increase in the following order: Pt/C > Ru/C > Pd/C > Fe/C > Ni/C > Co/C. However the overpotential of Pt/C for the HER is significantly larger (479 mV at 50 mA cm^{-2}) than its theoretical potential (−0.018 V, Fig. 2B and Fig. S5A, ESI†). Given the low overpotential (<100 mV) typically observed in H_2O(l) electrolysis with a Pt/C cathode,[19] the high overpotential in NH_3(l) electrolysis is attributed to the limited H^+ dissociation from NH_4^+ ($NH_4^+ \rightarrow NH_3 + H^+$) on the Pt surface. The released proton adatoms quickly generate H_2, as evidenced by the low Tafel slope (121 mV dec^{-1}, Fig. S5B, ESI†). Thus, incorporating metals (Ni, Co or Mo, *etc.*), known to promote H^+ dissociation from NH_4^+, into Pt metals could potentially reduce the HER overpotential.[31] Based on the screened results, we perform additional electrochemical characterizations using a Ru (anode)‖Pt (cathode) configuration with a 1 M NH_4Br electrolyte. Compared with the Ru‖Ru configuration, the NER overpotential shifts to 775 mV at 50 mA cm^{-2} (Fig. 2C and Fig. S6, ESI†). Likewise, the HER overpotential decreases to its theoretical value compared with that of the Pt‖Pt configuration (Fig. 2D and Fig. S7, ESI†). The results are likely attributed to improved electrochemical properties of each component arising from a decrease in solution resistance (R_s) (Fig. S8, ESI†). To promote catalytic activity in the Ru‖Pt configuration, additional NH_3(l) electrolysis is performed by increasing the concentration of the supporting electrolyte from 1 to 5 and 10 M. The electrochemical properties of the anode are slightly improved, reducing the

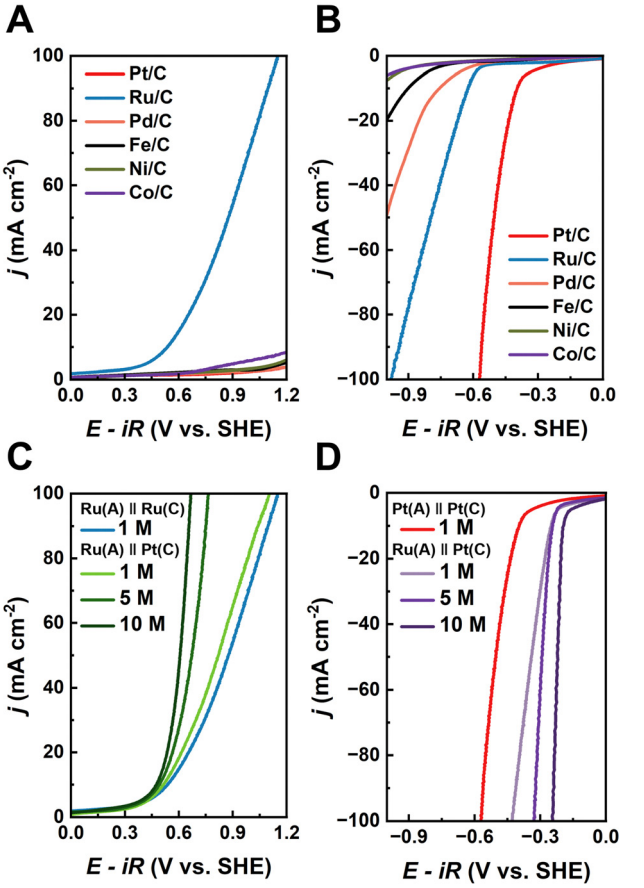

Fig. 2 **Electrochemical characteristics of the as-prepared catalysts determined by linear sweep voltammetry (LSV) with a scan rate of 5 mV s^{-1} under liquid anhydrous NH_3 (NH_3(l)) conditions at 10 °C and 6.2 bar**. (A) and (B) LSVs of the nitrogen evolution reaction (NER) and hydrogen evolution reaction (HER), respectively, using an electrode configuration with identical metals (M‖M, 2.5 μmol cm^{-2}) at both the anode and cathode in 1 M NH_4Br/NH_3(l) (see also Fig. S3 and S5, ESI†). (C) LSVs of the NER over Ru‖Ru in 1 M NH_4Br and Ru‖Pt configurations in 1 M, 5 M and 10 M NH_4Br (see also Fig. S6, ESI†). (D) LSVs of the HER over Pt‖Pt in 1 M NH_4Br and Ru‖Pt configurations in 1 M, 5 M and 10 M NH_4Br (see also Fig. S7, ESI†).

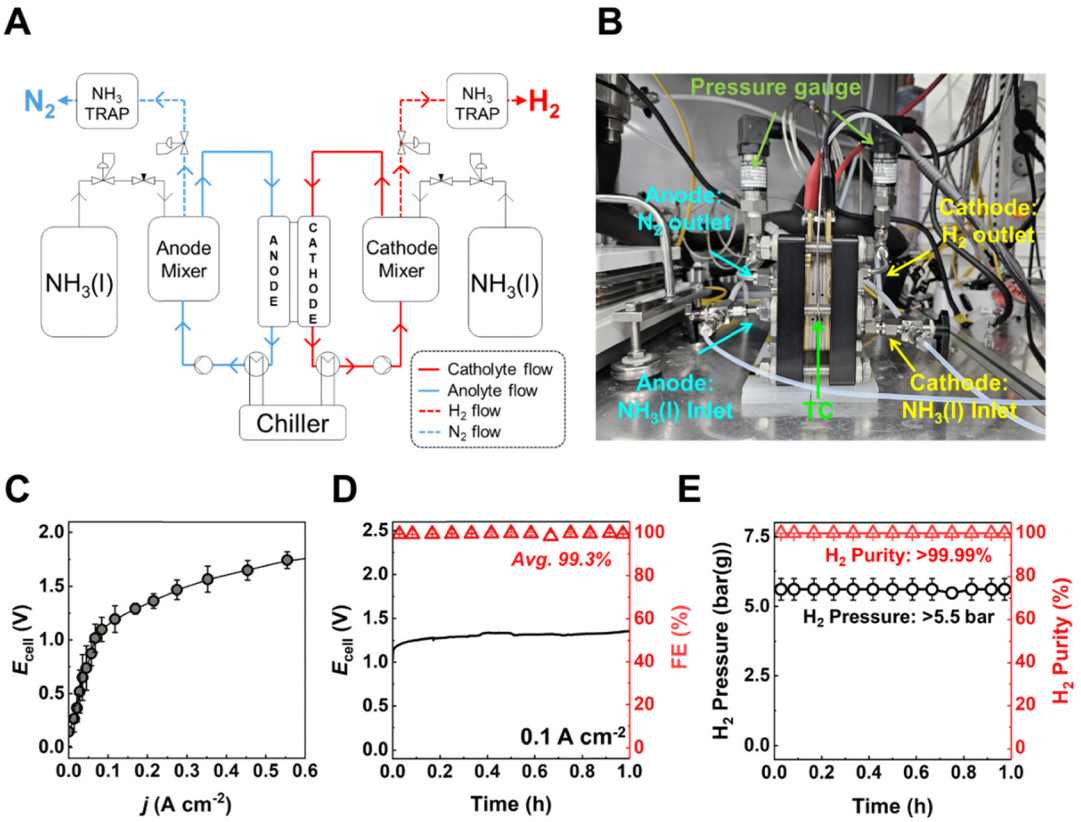

Fig. 3 **Continuous production of high-purity, pressurized H_2 using the as-designed NH_3(l) electrolyzer**. (A) Process flow diagram (PFD) of the as-designed NH_3(l) electrolysis system. (B) Digital photograph of the NH_3(l) electrolyzer (see also Fig. S10, ESI†). (C) *I–V* polarization characteristics of the NH_3(l) electrolyzer (anode: 2.5 μmol cm^{-2} of Ru/C, cathode: 2.5 μmol cm^{-2} of Pt/C) are determined with a scan rate of 5 mA s^{-1} at a flow rate of 30 mL min^{-1} and 10 °C, 6.2 bar conditions with 5 M NH_4Br. (D) Potential response of chronopotentiometry measured at 0.1 A cm^{-2} and Faradaic efficiency for H_2 production during electrolysis. (E) Purity and pressure of H_2 produced (see also Fig. S11, ESI†).

overpotential (η) at 50 mA cm^{-2} from 775 mV at 1 M to 625 mV at 5 M and 561 mV at 10 M (Fig. S6A, ESI†). In addition, the rate of the NER is further improved, as evidenced by a lower Tafel slope (237 mV dec^{-1} at 10 M) (Fig. 2C and Fig. S6B, ESI†). The enhanced activity is also associated with the lowering of the charge transfer resistance (R_{ct}) as shown by the Nyquist plot obtained from electrochemical impedance spectroscopy (EIS) (Fig. S8A, ESI†): 5.1 Ω at 1 M, 2.5 Ω at 5 M and 2.1 Ω at 10 M. To determine whether the bromide anion (Br^-) from the supporting electrolyte participated in the NH_3(l) electrolysis, we conducted an additional experiment using NH_4PF_6 as the supporting electrolyte, in which PF_6^- functions as an electrochemically inert anion. The resulting LSV profiles using NH_4PF_6 showed negligible differences compared to those obtained with NH_4Br (Fig. S9, ESI†). These results strongly suggest that the Br^- was inactive in the anodic process and did not contribute to the formation of byproducts such as Br_2 ($2Br^- \rightarrow Br_2 + 2e^-$). Conversely, Pt/C at the cathode exhibits a gentler Tafel slope (40 mV dec^{-1} at 10 M *vs.* 90 mV dec^{-1} at 1 M) with an overpotential of 202 mV at 50 mA cm^{-2} in 10 M of electrolyte (Fig. 2D and Fig. S7, ESI†). These results indicate that the enhanced charge and mass transfers under the high concentration of NH_4Br only slightly influence H^+ dissociation from NH_4^+, which could likely be the rate-determining step in the HER. Unlike the HER catalyst used in H_2O(l) electrolysis, developing alternative cathode materials for the HER in NH_3(l) electrolysis is necessary.

To evaluate the practical feasibility of the NH_3(l) electrolysis concept for extracting high-purity H_2, a continuous H_2 production system with a 25 cm^2 zero-gap type electrolysis cell is constructed (Fig. 3A, B and Fig. S10, ESI†). The NH_3(l) electrolyzer comprises Ru/C as the anode and Pt/C as the cathode, with a cationic exchange membrane. In the continuous electrochemical cell, NH_3(l) is mixed with the NH_4Br electrolyte, and the resulting 5 M NH_4Br/NH_3(l) solution is supplied to both the anode and cathode at 10 °C and 6.2 bar. During the reaction, unreacted NH_3(l) is recirculated into the mixer, and the produced H_2 and N_2 gases, along with less than 1% residual NH_3(g), are purified through an NH_3(g) trap (Fig. 3A). The *I–V* characteristic of the NH_3(l) electrolysis system shows a cell potential (E_{cell}) of *ca.* 1.1 V at 0.1 A cm^{-2} and *ca.* 1.6 V at 0.5 A cm^{-2} (Fig. 3C). This suggests that H_2 production is achievable at a lower potential than the cell potential of *ca.* 1.4 V at 0.1 A cm^{-2} for H_2O(l) electrolysis.[32,33] Despite this advantage, the NH_3(l) electrolysis system still exhibits a much higher cell potential than its theoretical value (0.068 V). Based on the results from both batch and flow electrolysis (Fig. 2 and 3, respectively), the high cell voltage is primarily attributed to activation polarization, while ohmic polarization and concentration overpotential are

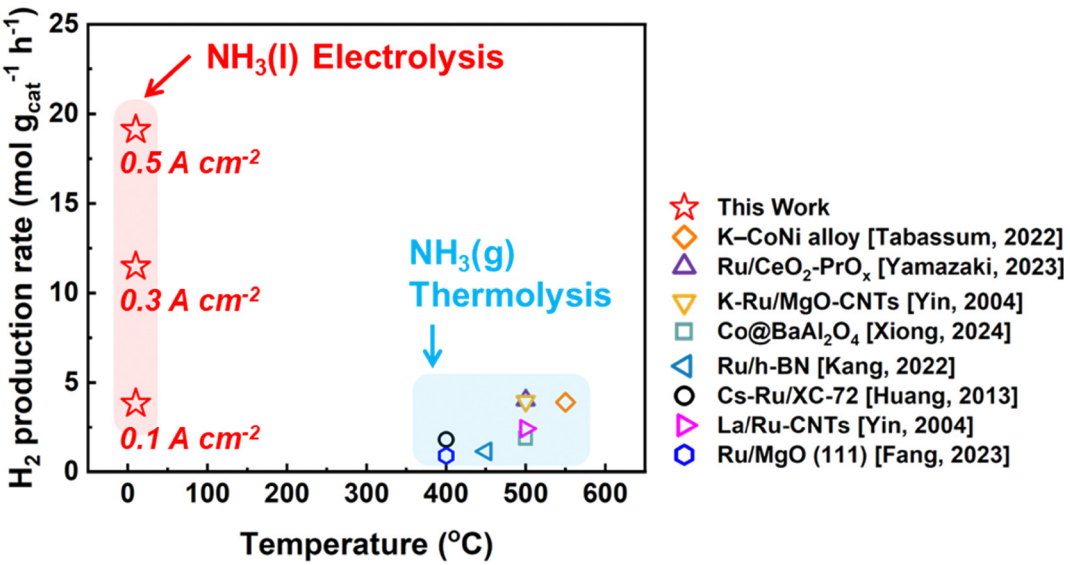

Fig. 4 **Comparison of H_2 production rate (mol g_{cat}^{-1} h^{-1}) obtained by NH_3(l) electrolysis and NH_3(g) thermolysis**. The unit mass of a catalyst for NH_3(l) electrolysis is defined as the mass of the catalyst of the cathode (12.2 mg of Pt/C).

considered negligible. To further determine the efficiency of H_2 production, NH_3(l) electrolysis is conducted at a constant current density of 0.1 A cm^{-2} for 1 h. The cell voltage remains below 1.3 V while maintaining a high Faradaic efficiency (FE) of 99.3% (Fig. 3D and Note S4, ESI†). Since only N_2 is detected at the anode and only H_2 at the cathode, it confirms the complete separation of hydrogen from N_2 and NH_3, with the H_2 purity exceeding 99.99% (Fig. 3E and Fig. S11, ESI†). The high-purity, pressurized H_2 (>5.5 bar) can be directly connected to a fuel cell without the need for additional pressure-boosting facilities.[34] Compared to previously reported batch type systems, the present NH_3(l) electrolysis system, designed in a zero-gap configuration, enables continuous production of high purity H_2 and demonstrates significantly enhanced activity for H_2 generation (Table S2, ESI†).

Finally, the rates of H_2 production *via* NH_3(l) electrolysis as a function of current density (j) are compared with those of reported thermal NH_3(g) decomposition systems (Fig. 4).[6,35–41] The as-designed NH_3(l) electrolysis system produces high-purity and pressurized H_2 continuously at 10 °C at a rate of 3.8 mol-H_2 g_{cat}^{-1} h^{-1} with a current density (j) of 0.1 A cm^{-2}, which is comparable to that of state-of-the-art NH_3(g) thermolysis (4.0 mol-H_2 g_{cat}^{-1} h^{-1}) at 500 °C and 1 bar.[35] When the operating current density is increased to 0.5 A cm^{-2}, an FE of 98.8% is achieved and the rate of H_2 release further increases to 18.8 mol-H_2 g_{cat}^{-1} h^{-1}, which is 4.7-fold higher than that of the aforementioned NH_3(g) thermolysis (4.0 mol-H_2 g_{cat}^{-1} h^{-1}).[35] Additionally, >98% of the initial NH_4Br electrolyte is recovered after two cycles (195.9 g → 192.0 g) and reused with negligible activity loss (Fig. S12, ESI†).

Conclusion

In this proof-of-concept study, to the best of our knowledge, we first demonstrate continuous H_2 production *via* direct electrolysis of anhydrous NH_3(l) at 10 °C under 6.2 bar without a high-cost separation process. Potential catalysts for NH_3(l) electrolysis are initially screened, with Ru/C (anode) and Pt/C (cathode) showing better activities than other metal catalysts. Based on the results, a continuous NH_3(l) electrolysis system equipped with a 25 cm^2 zero-gap cell and a cationic exchange membrane is designed. This system demonstrates high-purity and pressurized, continuous H_2 production at a rate of 18.8 mol-H_2 g_{cat}^{-1} h^{-1}, achieving an FE of >98.8% at 0.5 A cm^{-2}. This electrochemical cell has the potential to replace the thermochemical NH_3(g) decomposition systems currently under development, which require multiple separation processes (*e.g.*, temperature swing adsorption, pressure swing adsorption) and pressurizing components; moreover, the developed system holds significant promises for various commercial applications, particularly as an initial solution for small-scale and decentralized H_2 production facilities utilizing NH_3 (Table S3, ESI†). Despite these advantages, the obtained cell potential is higher than the theoretical value of 0.068 V. To lower the cell voltage, reducing the cathodic overpotential, enhancing the anodic N_2 evolution rate, stability of the electrocatalysts, developing cationic and/or anionic membranes for NH_3(l) electrolysis and improving system durability are essential.

Experimental section

Materials

Commercial active metal species (20% Pt, Ru, Pd, Fe, Co and Ni on Vulcan XC-72 conductive carbon black) were purchased from Premetek (Cherry Hill, NJ, US). Nafion solution (5 wt%, DS520) was obtained from Dupont (Wilmington, Delaware, US). Carbon paper (GDS210) for the batch experiment and carbon foam with a gas diffusion layer (EQ-bcgdl-1400S-LD) for the cell test were purchased from CeTech (Taichung, Taiwan) and MTI Korea (Seoul, South Korea), respectively. The cation exchange

membrane was purchased from Solvay (Aquivion E98-09S Brussels, Belgium), and its properties are listed as follows: thickness, 90 μm; tensile stress (MD: Break), 40 MPa; tensile stress (TD: Break), 30 MPa. Isopropanol (anhydrous, 99.5%) and NH_4Br (ACS reagent, ≥99.0%) were purchased from Sigma-Aldrich (St. Louis, MO, US) and used without further purification. Deionized water (DI·H_2O) was purified to a resistance of over 18 MΩ cm^{-1} using a water purification system (Pure ROUP 30, Purewater, Gyeong-gi, South Korea). NH_3(l) was supplied from a siphon tank at a purity of >99.99% (free of water and solvent).

Electrode fabrication

To screen the activities of different metals for the NER and HER, the commercial metals (M = Pt, Ru, Pd, Fe, Co and Ni) on carbon (C, Vulcan XC-72) are loaded on the carbon paper by the slurry coating method. **In a typical batch experiment**, an active metal amount is set to 2.5 μmol cm^{-2}. First, a metal precursor is initially dissolved in 530 μL of the mixture of isopropanol (IPA) and DI H_2O (1 : 1, vol%), and 100 μL of Nafion solution is added to the IPA/H_2O solution as a binder, making a total 630 μL. This precursor solution is then sonicated for 1 h to produce a well-dispersed solution, referred to as an 'ink'. Next, 31.5 μL of the ink is dropped onto 1 cm^2 of carbon paper to fabricate the electrode for screening the activities. Then, the prepared electrodes are dried in a vacuum for 30 min at 25 °C. **For full-cell operation**, the metal loadings for the NER and HER electrodes are also maintained at 2.5 μmol cm^{-2} (the total weight of Ru/C, 6.3 mg) for the anode and 2.5 μmol cm^{-2} (the total weight of Pt/C, 12.2 mg) for the cathode, respectively. The ink solution containing the mixture of IPA and DI H_2O (1 : 1, vol%, 2.12 mL) and 5 wt% Nafion solution (400 μL) is prepared. Next, 78.8 μL of the ink is dropped onto 25 cm^2 of carbon foam and then dried in a vacuum for 30 min at 25 °C.

Electrochemical measurements in the batch reactor

Electrochemical analyses for active metal screening are conducted using a high-pressure three-electrode batch reactor at 10 °C and 6.2 bar (specific cell configuration in Fig. S1, ESI†) with the addition of the supporting electrolyte (NH_4Br, 0–10 M). The Ag/AgCl (3.4 M KCl, Innovative Instruments, Inc., Tampa, FL, US) reference electrode, covered with polyetheretherketone (PEEK), along with the working and counter electrodes, is connected to a potentiostat (VSP with 4A booster; Bio-Logic Science Instruments, Seyssinet-Pariset, France) for electrochemical measurements. Prior to an experiment, the reactor is purged with Ar for 1 h to remove residual air. NH_3(l) is then supplied from a siphon-type container to the reactor, and a liquid regulator is used to maintain the reaction pressure at 6.2 bar. The applied potential is recalculated based on experimental conditions, with further details provided in Notes S1–S3 (ESI†). Analyses with linear sweep voltammetry (LSV) are performed at a scan rate of 5 mV s^{-1}, with the scan direction selected properly for each half-reaction: an oxidative sweep for the anodic reaction (NER) and a reductive sweep for the cathodic reaction (HER). Before conducting an experiment, 85% *iR* compensation was applied using the value of solution resistance (R_s) estimated from electrochemical impedance spectroscopy (EIS). To ensure an improved evaluation of intrinsic kinetics, the remaining 15% of uncompensated resistance was additionally corrected. The Nyquist plot from the EIS is obtained from 100 kHz to 100 MHz at +1.0 V_{SHE} for the anode and −1.2 V_{SHE} for the cathode. Tafel plots are calculated along the linear portion of the LSV.

Electrochemical measurements in the full-cell

Before an experiment, the NH_3(l) electrolyzer is purged with Ar for 1 h to remove residual air. In a typical electrolysis experiment, NH_3(l) and the supporting electrolyte (5 M NH_4Br) are initially homogenized using a magnetic stirrer in the anode and cathode mixers (200 mL) (refer to Fig. 3A). The resulting solutions are then supplied into the anode and cathode at a flow rate of 30 mL min^{-1}, followed by continuous circulation for 3 h to stabilize the cell. This procedure allows both the anode, cathode and membrane to be fully wet by NH_3(l). Note that the Aquivion membrane, which features perfluorosulfonic acid (PFSA) functionality, is reported to exhibit NH_4^+ conductivity of *ca.* 30 mS cm^{-1},[42] making it suitable for the purpose of this study.[43–47] The 25 cm^2 zero-gap type electrolyzer is operated at 10 °C and 6.2 bar using a DC power supply XG 20-76 (20 V, 76 A, Ametek, Berwyn, PA, US) with the current sweep (scan rate: 5 mA s^{-1}) and constant current methods. After the NH_3(l) splitting reaction, unreacted NH_3(l) is pumped back to each mixer for reuse. Finally, the obtained H_2 and N_2 gases are analyzed using a mass flow meter (F-201C; Bronkhorst, Ruurlo, Netherlands) and gas chromatography (YL6500; Young-In Chromass, Gyeong-gi, South Korea). Specific cell configuration and process flow diagrams are shown in Fig. 3A and Fig. S10 (ESI†).

Author contributions

Conceptualization, S. H., C. H. L. and C. W. Y.; methodology, S. H., J. S. H., H. L., C. H. L. and C. W. Y.; investigation, S. H. and H. L.; writing – original draft, S. H. and C. W. Y.; validation, J. S. H., J. S. L., C. H. L. and K. C. and C. W. Y.; writing – review and editing, S. H., J. S. H., J. S. L., H. L., C. H. L., K. C. and C. W. Y.; project administration, C. H. L., K. C. and C. W. Y.; funding acquisition, C. W. Y.; supervision, C. W. Y.

Data availability

The data supporting this article have been included as part of the ESI.†

Conflicts of interest

The authors declare no competing financial interest.

Acknowledgements

The authors gratefully acknowledge the support from the National Research Foundation of Korea (NRF, grant number

RS-2024-00421181) and the National Research Council of Science & Technology of Korea (NST, grant number GTL24051-200) funded by the Ministry of Science and ICT, Republic of Korea.

References

1 L. Schlapbach and A. Züttel, *Nature*, 2001, **414**, 353–358.
2 F. Chang, W. Gao, J. Guo and P. Chen, *Adv. Mater.*, 2021, **33**, 2005721.
3 U. B. Demirci and P. Miele, *Energy Environ. Sci.*, 2011, **4**, 3334–3341.
4 E. Spatolisano, L. A. Pellegrini, A. R. de Angelis, S. Cattaneo and E. Roccaro, *Ind. Eng. Chem. Res.*, 2023, **62**, 10813–10827.
5 F. Restelli, E. Spatolisano, L. A. Pellegrini, A. R. De Angelis, S. Cattaneo and E. Roccaro, *Int. J. Hydrogen Energy*, 2024, **52**, 532–547.
6 S. Kang, J. Cha, Y. S. Jo, Y. J. Lee, H. Sohn, Y. Kim, C. K. Song, Y. Kim, D. H. Lim, J. Park and C. W. Yoon, *Adv. Mater.*, 2023, **35**, 2203364.
7 D. R. MacFarlane, P. V. Cherepanov, J. Choi, B. H. Suryanto, R. Y. Hodgetts, J. M. Bakker, F. M. F. Vallana and A. N. Simonov, *Joule*, 2020, **4**, 1186–1205.
8 S. Sayas, N. Morlanés, S. P. Katikaneni, A. Harale, B. Solami and J. Gascon, *Catal. Sci. Technol.*, 2020, **10**, 5027–5035.
9 S. Chatterjee, R. K. Parsapur and K.-W. Huang, *ACS Energy Lett.*, 2021, **6**, 4390–4394.
10 D. Tang, G.-L. Tan, G.-W. Li, J.-G. Liang, S. M. Ahmad, A. Bahadur, M. Humayun, H. Ullah, A. Khan and M. Bououdina, *J. Energy Storage*, 2023, **64**, 107196.
11 Y. Yang, J. Kim, H. Jo, A. Seong, M. Lee, H.-K. Min, M.-G. Seo, Y. Choi and G. Kim, *J. Mater. Chem. A*, 2021, **9**, 11571–11579.
12 M. Cooper and G. G. Botte, *J. Electrochem. Soc.*, 2006, **153**, A1894.
13 J. Gwak, M. Choun and J. Lee, *ChemSusChem*, 2016, **9**, 403–408.
14 N. Akagi, K. Hori, H. Sugime, S. Noda and N. Hanada, *J. Catal.*, 2022, **406**, 222–230.
15 D. J. Little, M. R. SmithIII and T. W. Hamann, *Energy Environ. Sci.*, 2015, **8**, 2775–2781.
16 N. Hanada, S. Hino, T. Ichikawa, H. Suzuki, K. Takai and Y. Kojima, *Chem. Commun.*, 2010, **46**, 7775–7777.
17 B.-X. Dong, T. Ichikawa, N. Hanada, S. Hino and Y. Kojima, *J. Alloys Compd.*, 2011, **509**, S891–S894.
18 A. J. Shih, M. C. Monteiro, F. Dattila, D. Pavesi, M. Philips, A. H. da Silva, R. E. Vos, K. Ojha, S. Park and O. van der Heijden, *Nat. Rev. Methods Primers*, 2022, **2**, 84.
19 M. Chatenet, B. G. Pollet, D. R. Dekel, F. Dionigi, J. Deseure, P. Millet, R. D. Braatz, M. Z. Bazant, M. Eikerling, I. Staffell, P. Balcombe, Y. Shao-Horn and H. Schäfer, *Chem. Soc. Rev.*, 2022, **51**, 4583–4762.
20 K. Siddharth, Y. Chan, L. Wang and M. Shao, *Curr. Opin. Electrochem.*, 2018, **9**, 151–157.
21 C. Zhong, W. Hu and Y. Cheng, *J. Mater. Chem. A*, 2013, **1**, 3216–3238.
22 X. Ding, Y. Ji, H. Huang, J. Huang, S. Chen, C. Yang, F. Li and M. Luo, *Chem. Catal.*, 2024, **4**, 100932.
23 A. Allagui, M. Oudah, X. Tuaev, S. Ntais, F. Almomani and E. A. Baranova, *Int. J. Hydrogen Energy*, 2013, **38**, 2455–2463.
24 N. S. Hassan, A. A. Jalil, R. Saravanan, N. M. Izzuddin, M. B. Bahari, D. Prasetyoko and R. E. Nugraha, *J. Mater. Chem. A*, 2024, **12**, 23202–23217.
25 L. Carmichael and B. Sage, *Ind. Eng. Chem. Res.*, 1952, **44**, 2728–2732.
26 D. Kong, C. Meng, Y. Wang, X. Chen, J. Zhang, L. Zhao, J. Ji, L. Zhang and Y. Zhou, *Appl. Catal., B*, 2024, **343**, 123578.
27 Y. Gorlin and T. F. Jaramillo, *J. Am. Chem. Soc.*, 2010, **132**, 13612–13614.
28 D. J. Little, D. O. Edwards, M. R. Smith III and T. W. Hamann, *ACS Appl. Mater. Interfaces*, 2017, **9**, 16228–16235.
29 F. García-García, A. Guerrero-Ruiz and I. Rodríguez-Ramos, *Top. Catal.*, 2009, **52**, 758–764.
30 J. C. Ganley, F. Thomas, E. Seebauer and R. I. Masel, *Catal. Lett.*, 2004, **96**, 117–122.
31 D. A. Hansgen, D. G. Vlachos and J. G. Chen, *Nat. Chem.*, 2010, **2**, 484–489.
32 L. Tao, F. Lv, D. Wang, H. Luo, F. Lin, H. Gong, H. Mi, S. Wang, Q. Zhang and L. Gu, *Joule*, 2024, **8**, 450–460.
33 Y. Hong, S. C. Cho, S. Kim, H. Jin, J. H. Seol, T. K. Lee, J.-K. Ryu, G. M. Tomboc, T. Kim and H. Baik, *Adv. Energy Mater.*, 2024, **14**, 2304269.
34 J. Hoeflinger and P. Hofmann, *Int. J. Hydrogen Energy*, 2020, **45**, 29246–29258.
35 K. Yamazaki, M. Matsumoto, M. Ishikawa and A. Sato, *Appl. Catal., B*, 2023, **325**, 122352.
36 S. Yin, B. Xu, S. Wang, C. Ng and C. Au, *Catal. Lett.*, 2004, **96**, 113–116.
37 D.-C. Huang, C.-H. Jiang, F.-J. Liu, Y.-C. Cheng, Y.-C. Chen and K.-L. Hsueh, *Int. J. Hydrogen Energy*, 2013, **38**, 3233–3240.
38 S.-F. Yin, B.-Q. Xu, C.-F. Ng and C.-T. Au, *Appl. Catal., B*, 2004, **48**, 237–241.
39 P. Xiong, Z. Xu, T.-S. Wu, T. Yang, Q. Lei, J. Li, G. Li, M. Yang, Y.-L. Soo, R. D. Bennett, S. P. Lau, S. C. E. Tsang, Y. Zhu and M. M.-J. Li, *Nat. Commun.*, 2024, **15**, 420.
40 H. Fang, S. Wu, T. Ayvali, J. Zheng, J. Fellowes, P.-L. Ho, K. C. Leung, A. Large, G. Held, R. Kato, K. Suenaga, Y. I. A. Reyes, H. V. Thang, H.-Y. T. Chen and S. C. E. Tsang, *Nat. Commun.*, 2023, **14**, 647.
41 H. Tabassum, S. Mukherjee, J. Chen, D. Holiharimanana, S. Karakalos, X. Yang, S. Hwang, T. Zhang, B. Lu, M. Chen, Z. Tang, E. A. Kyriakidou, Q. Ge and G. Wu, *Energy Environ. Sci.*, 2022, **15**, 4190–4200.
42 J. Peng, K. Lou, G. Goenaga and T. Zawodzinski, *ACS Appl. Mater. Interfaces*, 2018, **10**, 38418–38430.
43 L. Xu, D. Liu, W. Liu, J. Yang, J. Huang, X. Wang and Q. He, *ACS Omega*, 2022, **7**, 20634–20643.
44 R. Lan and S. Tao, *ECS Electrochem. Lett.*, 2013, **2**, F37.
45 V. Signorini, A. Askin, C. Oldani, M. Minelli and M. Giacinti Baschetti, *J. Membr. Sci.*, 2024, **697**, 122564.
46 Y. He and E. L. Cussler, *J. Membr. Sci.*, 1992, **68**, 43–52.
47 K. Wakimoto, W.-W. Yan, N. Moriyama, H. Nagasawa, M. Kanezashi and T. Tsuru, *J. Membr. Sci.*, 2022, **658**, 120718.